Supplementary Information for

Nonlinear Nonlocal Metasurfaces

Michele Cotrufo[1,2,†], Luca Carletti[3,4,†], Adam Overvig[1,5], and Andrea Alù[1,6,#,*]

[1]*Photonics Initiative, Advanced Science Research Center, City University of New York, New York, NY 10031, USA*

[2]*The Institute of Optics, University of Rochester, Rochester, New York 14627, USA*

[3]*Department of Information Engineering, University of Brescia, Via Branze 38, 25123, Brescia, Italy*

[4]*National Institute of Optics – National Research Council (INO-CNR), Via Branze 45, 25123, Brescia, Italy*

[5]*Department of Physics, Stevens Institute of Technology, Hoboken, NJ 07030, USA*

[6]*Physics Program, Graduate Center of the City University of New York, New York, NY 10016, USA*

[†] *These authors contributed equally*

**aalu@gc.cuny.edu*

Table of Contents

Section S1. Raw data of the THG Fourier Imaging

In Fig. 3a of the main text we showed the experimentally measured k-space TH emission for different combinations of pump polarizations and TH polarization component. The experimental data in Fig. 3a was shown as histograms, where each two-dimensional bin corresponds to a certain TH diffraction order. The corresponding raw data is shown here in Fig. S1. The twelve panels of Fig. S1 show the raw Fourier images acquired by the CCD camera (with the setup shown in Fig. 5 of the main text), for different combinations of pump polarizations (indicated at the left of each row) and TH polarization component (indicated at the top of each column). The arrangement of the panels in Fig. S1 matches the structure of Fig. 3a of the main paper. In order to aid comparison between different measurements, each intensity map in Fig. S1 has been normalized by the acquisition time of the camera and by the cube of the pump power.

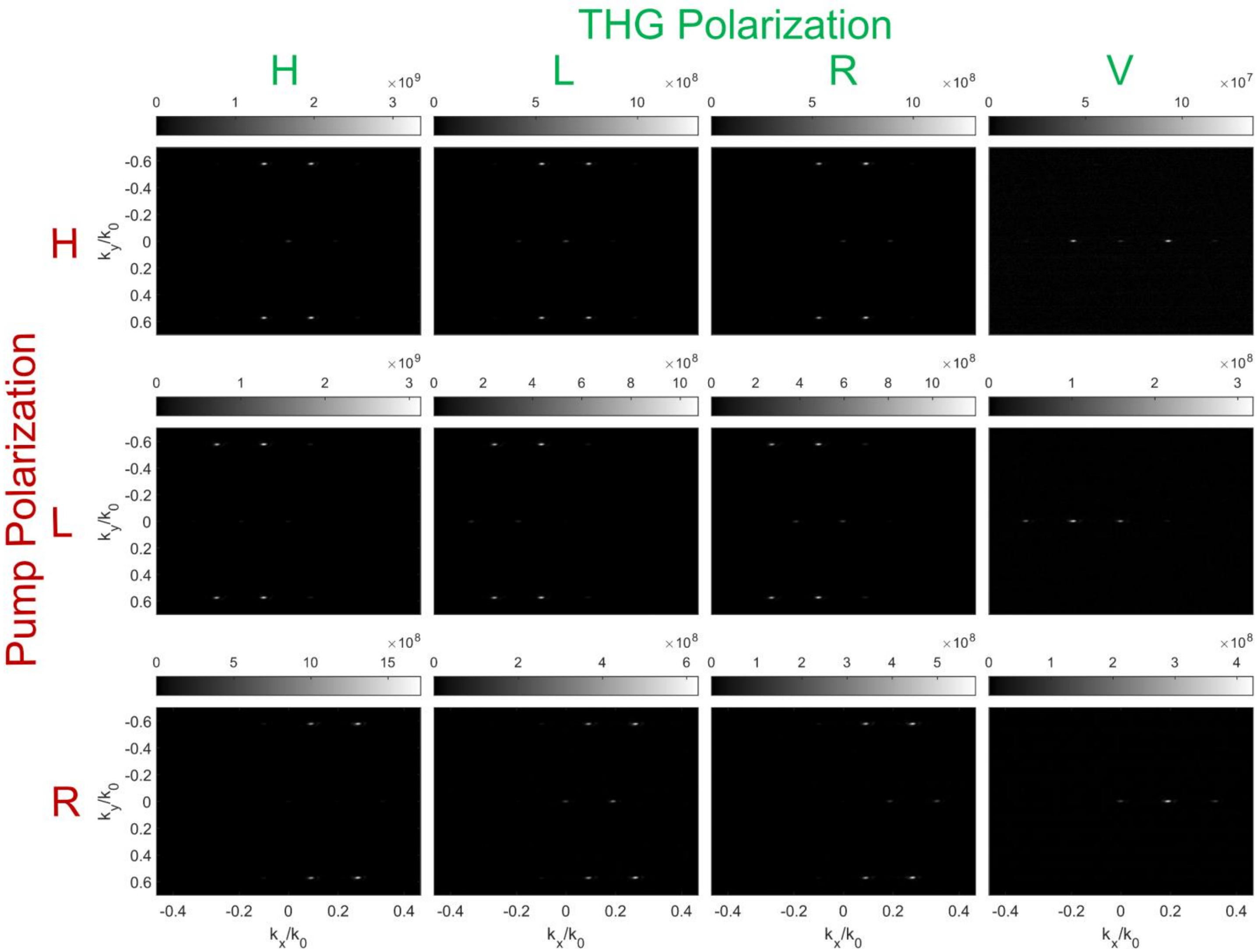

Figure S1. Raw experimental data used to obtain the histograms shown in fig. 3 of the main text. The data show the k-space emission of the third-harmonic signal for different combinations of pump polarization (reported on the left of each row) and third-harmonic polarization component (reported on the top of each row). H = horizontal, V = vertical, L = left circularly polarized, R = right circularly polarized. See text for additional details.

Section S2. Linear transmittance calculations

We used finite-element-method calculations implemented in COMSOL to numerically estimate the transmittance spectra of periodic metasurfaces for different values of ρ and polarized excitations. The transmittance spectra for linearly polarized light along the x-axis direction and y-axis direction are shown in Fig. S2(a) and S2(b). These spectra manifest opposite trend with respect to the in-plane rotation angle ρ of the rectangular apertures. In Fig. S3, the transmittance for right-circular polarized light is shown. We observe that the Fano-lineshape resulting from the resonance excitation appears for each angle ρ. Furthermore, we can observe that the lineshape spectrally blue-shifts when ρ goes from 0° to 45°, indicating a small detuning of the qBIC wavelength as ρ varies. This detuning causes a subsequent modulation of the THG efficiency as a function of ρ as it is observed in Fig. 1(f).

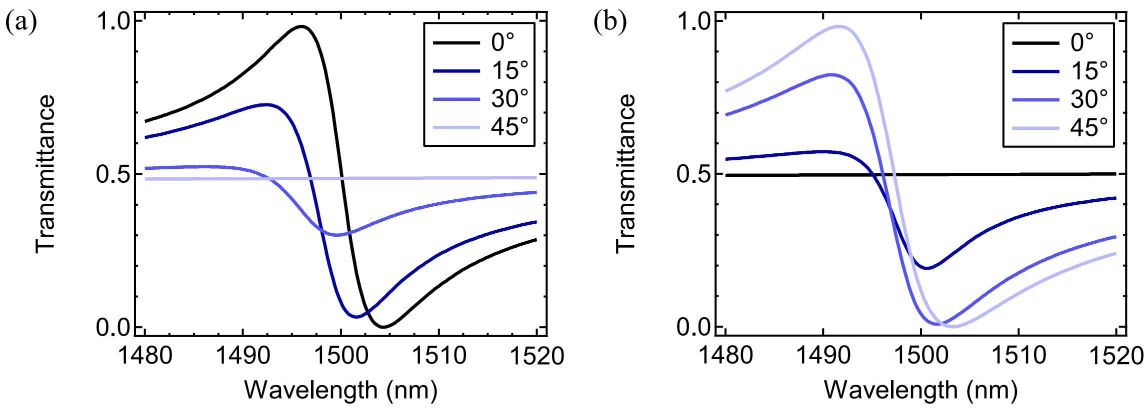

Figure S2. (a) x-polarized and (b) y-polarized transmittance spectrum of a periodic metasurface with unit cell in Fig. 1(a), as ρ changes from 0° to 45°.

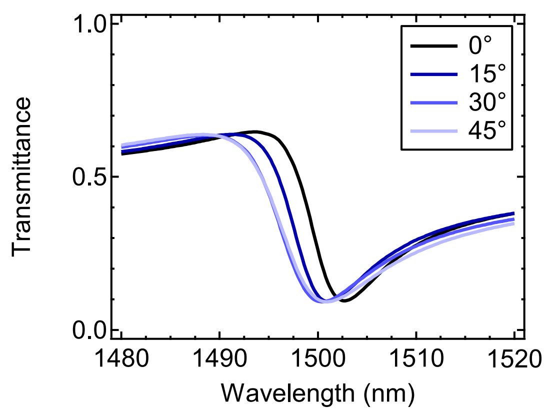

Figure S3. Right-circular polarized transmittance spectrum of a periodic metasurface with unit cell in Fig. 1(a), as ρ changes from 0° to 45°.

Section S3. Polarization properties of the THG emission from unit cell

We numerically analyzed the TH radiation pattern of the basic unit-cell of our design with angle ρ set to 0° for different states of pump polarization. Figure S4 reports the TH emission in the different diffractive orders for x-polarized, left-circularly polarized, and right-circularly polarized pump. The polarization ellipse of light emitted in each diffraction order is represented by a black curve. We can observe that, independently from the pump polarization, most of the TH is radiated in the (0,±1) diffraction orders.

Furthermore, the polarization state is mainly linear and oriented along the x-axis direction. This is due to the electric field distribution of the TH that is shown in Fig. 1(d) of the main text.

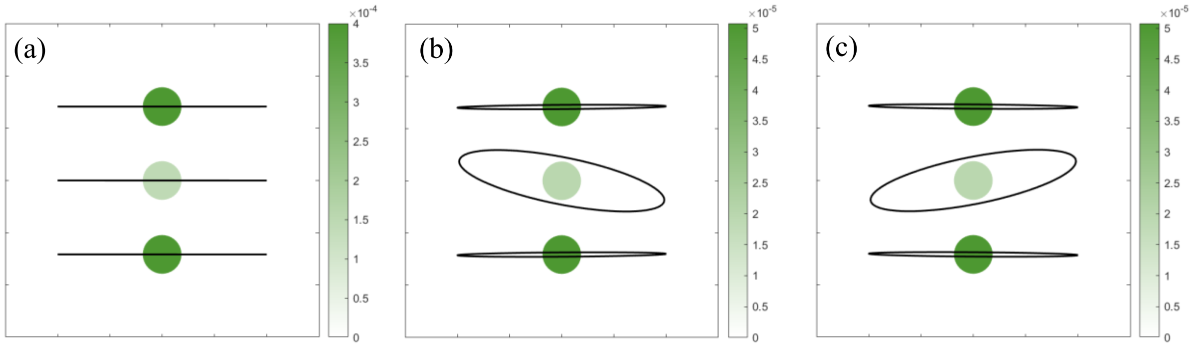

Figure S4. THG emission for (a) linearly x-polarized, (b) left-polarized, and (c) right-circularly polarized pump. Color represents intensity of the emission. Black lines represent polarization ellipses of each diffraction order.

Section S4. Comparison of state-of-the art THG with silicon-based metasurfaces.

Work	Resonance type	Pump wavelength (nm)	Wavefront control method	Pulse duration / Repetition rate	Pump power/intensity (either average or peak)	TH power/intensity (either average or peak)	Conversion efficiency	Normalized efficiency for Peak Power (1/W^2)
This Work	Nonlocal	1530	Geometric phase	2 ps / 80 MHz	1.6 KW (peak)	3.8 mW (peak)	$2.3 \cdot 10^{-6}$	$8.5 \cdot 10^{-13}$
[32] Advanced Science 2022, 9, 2104508	Local (MD)	1300	Geometric phase	200 fs / 80 MHz	100 mW (avg)	140 nW (avg)	$1.4 \cdot 10^{-6}$	$3.5 \cdot 10^{-14}$
[34] ACS Photonics 10, 4357--4366 (2023)	Nonlocal	1200	Geometric phase	200 fs / n.a.	n.a.	n.a.	$3.5 \cdot 10^{-9} \div 6.5 \cdot 10^{-8}$	n.a.
[29] Nano Lett. 2018, 18, 6, 3978–3984	Local	1615	Resonance tuning	300 fs / 20 MHz	200 mW (avg)	300 nW (avg)	$1.5 \cdot 10^{-6}$	$1.3 \cdot 10^{-15}$ †
Nano Lett. 2024, 24, 2257−2263	Local (Multipolar)	1320	Resonance tuning	100 fs / 10 KHz	24GW/cm^2 (peak)	n.a.	$3.25 \cdot 10^{-5}$	$3.1 \cdot 10^{-16}$ †
Nano Lett. 2020, 20, 6, 4370–4376	Local	1550	Resonance tuning	40 fs / 1 MHz	1.8 mW (avg)	n.a.	10^{-6}	$5 \cdot 10^{-16}$ †
Nano Lett. 2018, 18, 12, 8054–8061	Nonlocal (qBIC)	1400	Resonance tuning	100 fs / 1 KHz	33 GW/cm^2 (peak)	10^{-3} nJ (pulse energy)	$1.1 \cdot 10^{-6}$	$1.3 \cdot 10^{-20}$ †
Nano Lett. 2019, 19, 9, 6585–6591	Local (Multipolar)	1300	Geometric phase	200 fs / 80 MHz	5.2 KW (peak)	52 nW † (peak)	10^{-11}	$3.7 \cdot 10^{-19}$ †

Table S1. Comparison of the current state of the art of THG with silicon based metasurfaces with nonlinear warfront shaping capabilities. Experimentally reported values are compared. All values without a superscript annotation have been taken directly from the respective paper.
* Extracted from figures in the paper.
† Calculated based on data in the paper.
"n.a." = either not applicable or not mentioned in the paper.

Section S5. Impact of fabrication tolerances on the dimensions of the rods

The effects shown in Fig. 1c of the main paper are robust with respect to variations of the dimensions of the rods. We numerically verify this in Fig. S5 where we compare, for different values of ρ, the transmission spectrum of the ideal design with the ones obtained when the rod dimensions are varied by ± 10 nm. As it can be seen, such variations induce an overall spectral shift of the qBIC wavelength, but do not alter one of the fundamental mechanisms of our approach, that is, the fact that the coupling between the qBIC and the different free-space linear polarizations can be controlled by ρ.

Thus, if the fabrication imperfections result in a systematic variation of all geometrical features (i.e., all geometrical features are scaled by the same scale factor), the overall effect is simply a shift of the operational frequency, and we do not expect any major degradation on the desired phase profile. If the fabrication imperfections are randomly distributed such that, e.g., each unit cell is affected by a different scaling factor, we generally expect the phase profile to be distorted and the beam-steering efficiency to be worsened.

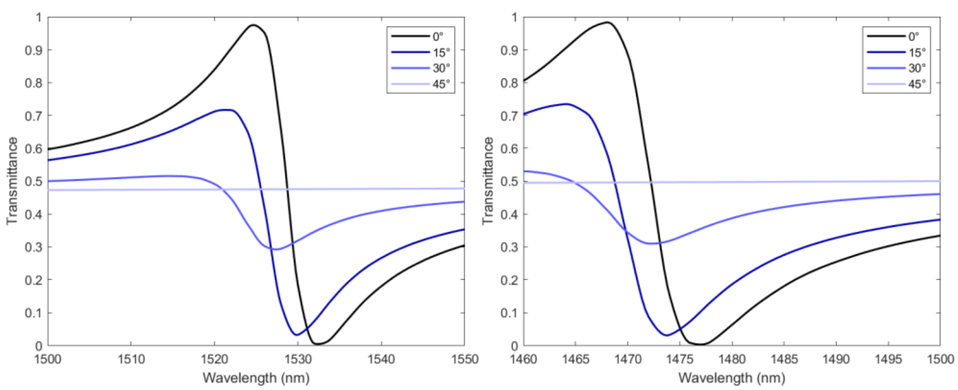

Figure S5. Transmittance spectra of the unit-cell where the dimensions W and L are changed by (a) -10 nm and (b) 10 nm as compared to the ones assumed in the simulations in Fig. 1 of the main paper and Figs. S2-S4.